




Application of Coal Fly Ash–Derived Zeolites for Batch Adsorption of Chromium from Wastewater

Tebogo Mphatlalala Mokgehle  ·
Funanani Bridget Nevhudogwa ·
Nikita Tawanda Tavengwa

Received: 19 November 2021 / Accepted: 4 July 2022 / Published online: 13 July 2022
© The Author(s), under exclusive licence to Springer Nature Switzerland AG 2022

Abstract The application of coal fly ash has for decades been regarded as a viable method for the adsorption of chromium in contaminated water. However, coal fly ash as an adsorbent has its setbacks due to its limited number of adsorption sites, resulting in inadequate extraction efficiencies. In this work, batch adsorption studies of chromium from wastewater were done using zeolites derived from coal fly ash. The hydrothermal treatment technique for synthesis of zeolites consisted of ageing and crystallization studies. The optimized conditions for ageing were a concentration of 2.5 M NaOH for the activating agent, aged for 48 h with the NaOH volume at 100 mL. Thereafter, crystallization studies were performed evaluating the effect of the H₂O/SiO₂ ratio, crystallization time and crystallization temperature, where the optimum conditions were observed at 1, 72 h and 200 °C, respectively. The adsorption performance of these materials was evaluated with respect to mass of zeolite, influent concentration, contact time and temperature, where the optimized parameters were 80 mg, 0.9 M, 420 min and 75 °C, respectively. In conclusion, application studies revealed that the chromium concentration in tap water from the

studied municipality was below the detection limit, indicating that the water was adequately treated.

Keywords Batch adsorption · Coal fly ash zeolites · Chromium · Wastewater · Remediation

1 Introduction

Pollution of the ecosystem due to toxic non-degradable heavy metals presents a serious health hazard (Doabi et al., 2018; Khan et al., 2021; Pakade et al., 2017). One such heavy metal is chromium, which exhibits toxicity by being able to penetrate biological cell membranes resulting in cancer (Deepak et al., 2021; Fu et al., 2020; Zhang et al., 2020). Chromium can be discharged in several ways some of which include industrial activities and natural causes such as volcanic eruptions, which lead to seepage of chromium compounds into the environment (Pakade et al., 2016; Rahman & Singh, 2019). Chromium has a variety of oxidation states. The rare oxidation states include '+1', '+4' and '+5' (Bansal et al., 2019; Farouk et al., 2020). The most common oxidation states include the trivalent Cr(III) and hexavalent Cr(VI) states (Park, 2020; Edwards et al., 2020). Hexavalent chromium is the most stable and persistent form of chromium in the environment (Zhao et al., 2018; Zhu et al., 2020). Hexavalent chromium is also the most toxic form of chromium as it is highly mobile and can easily pass through cell membranes,

T. M. Mokgehle · F. B. Nevhudogwa ·
N. T. Tavengwa (✉)

Department of Chemistry, Faculty of Science, Engineering and Agriculture, University of Venda, Private Bag X5050, Thohoyandou 0950, South Africa
e-mail: nikita.tavengwa@univen.ac.za

where it is reduced to Cr(III), making it carcinogenic, resulting in stomach ulcers and mitochondrial functional damage (Zhao et al., 2018; Bakshi & Panigrahi, 2018; Sadeghi et al., 2019; Noah et al., 2020; Zhu et al., 2020; Wang et al., 2021; Huang et al., 2022).

Agencies, such as the World Health Organisation (WHO), have set regulations for maximum tolerable concentration limits of 0.05 mg L^{-1} and 0.1 mg L^{-1} for Cr(VI) in drinking water and inland surface water, respectively (WHO, 2003; Maitlo et al., 2021). Furthermore, a local study by Edokpayi et al. (2018) reported that the carcinogenic risk due to Cr exposure, in a number of boreholes studied in Muledane village situated in Limpopo, South Africa, exceeded the $50\text{-}\mu\text{g L}^{-1}$ risk limit for chromium in drinking water as set by the Department of Water Affairs and Forestry (DWAFF) (1996) and WHO (2006) (Loock-Hattingh, 2016). Sources of pollution in various water bodies such as rivers, lakes and boreholes include discharge of wastewater from domestic, agricultural and industrial activities (Jalees et al., 2021; Buba & Maina, 2020). Other causes of pollution in groundwater sources include the geology of the aquifers, climate and anthropogenic activities (Edokpayi et al., 2018; Kurwadkar et al., 2020). Different techniques have been used for the removal of heavy metals which include ion exchange, solvent extraction and chemical precipitation (Alguacil et al., 2008; Bashir et al., 2019; Chen et al., 2018; Dong et al., 2018; Feng et al., 2019; Sorouraddin et al., 2017; Xie et al., 2019; Ye et al., 2019). These methods have been accompanied by setbacks; for instance, ion exchange often requires that concentrations of more species need to be measured to ascertain it (Crist et al., 2002), solvent extraction is generally expensive and is often results in poor extraction efficiencies (Nguyen & Lee, 2018), while chemical precipitation suffers from poor solubility of chromium sulphides and requires large doses of precipitation agents (Pohl, 2020). Adsorption with the use of a suitable adsorbent can be a more effective technique for the removal of heavy metals in aqueous systems (Saleh et al., 2020; Xiaodong et al., 2019). Ferric oxide (Son et al., 2018) and alumina (Chang et al., 2020) have been used as adsorbents for heavy metals due to their high adsorption capacity, but they are difficult to separate from the aqueous system after use and they are expensive. Therefore, there is a need to develop low cost and readily regenerative adsorbents.

Coal fly ash (CFA) is an example of a low-cost adsorbent, generated as a waste material during combustion of coal (Mokgehle et al., 2019a; Vu et al., 2020). The abundance of CFA makes it difficult to dispose. Due to the voluminous nature of CFA, stockpiled CFA during heavy rains leach heavy metal ions into water bodies contaminating and disrupting the ecosystem (Mokgehle et al., 2019b; Hwang et al., 2020). Some of the toxic effects of CFA include increased risk of developing cancer and other diseases (Whiteside & Herndon, 2018). Efforts have been undertaken to recycle CFA. Approximately, 20% of the CFA produced is being used as building material (Sanjuán et al., 2021). Despite the uses of CFA, a large portion of this material remains at landfill sites and still poses an environmental hazard. As a remediation strategy, CFA has therefore been studied as a sorbent for heavy metal ions (Lei et al., 2020; Xie et al., 2014). However, application of CFA in adsorption has often been accompanied by setbacks which include limited adsorption sites. To address these limitations and improve the adsorption performance, this work was directed at the application of hydrothermally treated CFA-derived zeolites for the adsorption of chromium via the batch technique. The hydrothermal synthesis method is suitable as it firstly uses a green solvent, water, for producing zeolites. Secondly, it is an appropriate method for using an abundant waste material (CFA) for synthesis of zeolites.

2 Experimental

2.1 Chemicals and Reagents

CFA was collected from a Modderfontein (Johannesburg, South Africa) steam plant. $\text{Al}_2(\text{SO}_4)_3 \cdot 18\text{H}_2\text{O}$ was purchased from Associated Chemical Enterprises (Johannesburg, South Africa), and SiO_2 was purchased from Sigma-Aldrich (Johannesburg, South Africa), which were used as standards in the analysis of dissolved Si^{4+} and Al^{3+} species. NaOH pellets, HNO_3 and $\text{K}_2\text{Cr}_2\text{O}_7$, were purchased from Rochelle Chemicals (Johannesburg, South Africa). The NaOH pellets were used as alkaline-activating agents for dissolution of the aluminosilicate matrix in CFA. Ultra-pure water was purified using a Direct-Q 5UV distiller (MA, USA) with a conductivity and resistance of $0.055 \mu\text{S cm}^{-1}$ and $18.2 \text{ m}\Omega$ respectively. A

magnetic stirrer was used to stir CFA and NaOH. Filtration was done using a filter paper to separate the slurry from the NaOH-activating solution.

2.2 Instruments

Analysis of the dissolved ions from the CFA aluminosilicate matrix were performed on a PinAAcle 900 T flame atomic absorption spectrometer (AAS), purchased from PerkinElmer (MA, USA). A Heidolph temperature probed magnetic stirrer from Heidolph Instruments (Schwarzenberg, Germany) was used to stir CFA and the alkaline activating solution. Filtration was done using a Millipore 0.2- μm membrane filter to separate the slurry from the NaOH-activating solution. A CN-2060 centrifuge acquired from Monitoring and Control Laboratories (Johannesburg, South Africa) was used to separate the slurry from the NaOH-activating solution. Analysis of the dissolved ions from the CFA aluminosilicate matrix was performed on a PinAAcle 900 T graphite furnace atomic absorption spectrometer (AAS) procured from PerkinElmer (MA, USA).

A 278AC Brass Parr Bomb purchased from the Parr Instrument Company (IL, USA) was used to perform crystallization of the CFA slurry. The Parr bomb was placed in a Labotec EcoTherm oven (Johannesburg, South Africa). Molecular interactions were characterized using Fourier transform infrared (FT-IR) spectroscopy from Bruker (MA, USA). A Bruker S1 Titan/Tracer XRF analyser (Cramerview, South Africa) was used to determine the chemical composition of the materials.

2.3 Ageing Studies

During ageing studies, the concentrations of 0.5–1.5 mol L⁻¹ NaOH were prepared. NaOH solutions were prepared and then mixed with 15 g CFA in a 250-mL polypropylene sealable bottles and stirred at 400 rpm for 24 h at 50 °C to determine the extent of dissolution of the CFA aluminosilicate matrix. After the stirring period had elapsed, the slurry was filtered. The filtrate was then analysed for Si⁴⁺ and Al³⁺ using FAAS. The next study evaluated the effect of ageing time where the optimized concentration of NaOH was used to determine the optimum time for complete dissolution of the CFA Al matrix into the activating agent. The optimized NaOH concentration,

50 mL, was mixed with 15 g CFA in a 250-mL polypropylene sealable bottle and stirred at 400 rpm for a variety of time intervals (6–48 h) at 50 °C. After the stirring periods had elapsed, the slurry was filtered. The filtrate was then analysed for Si⁴⁺ and Al³⁺ using FAAS. The concluding ageing study looked at the effect of the solid/liquid ratio. The optimized NaOH concentration and ageing time were used to investigate the dissolution of Si⁴⁺ and Al³⁺ as a function of solid/liquid ratio (0.15–0.5 g mL⁻¹). These mixtures were placed in 250-mL polypropylene sealable bottles and stirred at 400 rpm at 50 °C. After stirring, the slurry was filtered, and the filtrate was analysed for Si⁴⁺ and Al³⁺ content using a FAAS. Following the optimized ageing conditions, crystallization studies were conducted where the effect of crystallization time was examined.

2.4 Crystallization Studies

A 15-mL slurry from ageing studies in Sec 2.3 was poured into a parr bomb and crystallized in an oven at 140 °C for 6–72 h to form zeolites. Thereafter, temperature studies were conducted by pouring 15 mL slurry from the ageing studies, synthesized from the optimum conditions, into a parr bomb. This unit was then placed in an oven for crystallization at temperatures ranging from 35 to 200 °C under a period equivalent to the optimum time. Analyses were then done on the synthesized zeolites via XRF and FTIR. This was followed by a study evaluating the effect of water content on crystallization where the solid (slurry):liquid (water) ratios were 5:10, 7.5:7.5 and 15:0 (v/v). The mixtures were poured into the parr bomb and placed into an oven for crystallization. This was done under the optimum conditions of time and temperature. FT-IR analysis was then done on the resultant zeolites.

2.5 Adsorption of Chromium

Batch adsorption studies were then done evaluating the effect of mass of zeolite, which ranged from 10 to 80 mg, on the extraction of chromium. The conditions for chromium adsorption were 0.5 g mL⁻¹ Cr, at a stirring rate of 100 rpm at 25 °C for 3 h each. After the stirring period had elapsed, the mixture was filtered, and the filtrate was analysed for chromium using FAAS. The next batch study evaluated the

effect of contact time (30–420 min) which was performed using the optimum mass of zeolite from the previous study. After the stirring period had elapsed, the mixture was filtered, and the filtrate was analysed for chromium using FAAS. This was followed by the effect of concentration (0.1–0.9 mg L⁻¹) studies. The concluding study evaluated the effect of temperature (25–75 °C) on chromium adsorption. All the filtered solutions were analysed on the FAAS. All the adsorption experiments were conducted in duplicates.

3 Results and Discussion

3.1 Synthesis of Zeolite via Hydrothermal Treatment

3.1.1 Ageing Studies

Effect of Concentration of NaOH on the Dissolution of the Aluminosilicate Matrix of CFA.

The surface of the CFA particle was composed of a highly reactive aluminosilicate layer. The outer layer of CFA composed of the aluminosilicate layer was mainly made of SiO₂ while the aluminium content was concentrated in the interior, also referred to as the mullite layer. The trend observed amongst the three concentrations studied indicated that as the concentration of NaOH was increased, the dissolution of the CFA aluminosilicate layer into NaOH increased (Fig. 1) (Mokgehle et al., 2019a). The disproportionately larger concentration of Si⁴⁺ dissolved compared to Al³⁺, indicating that a large portion of CFA was composed of aluminosilicate, which had a high silica content. It was also observed that as the alkali concentration was increased, dissolution of Al³⁺ increased. This was mainly due to the high pH of the alkaline solution (1.5 M NaOH), which penetrated the inner

mullite phase resulting in an increased concentration of Al³⁺ compared to the 0.5-M and 1.0-M NaOH alkaline solutions (Fig. 1). Mokgehle et al. (2019a) and Inada et al. (2005) also reported on a similar trend. An optimum dissolution of 1.5 M NaOH was then used in subsequent experiments.

Effect of Time on the Dissolution of the Aluminosilicate Matrix of CFA

Studies were performed to investigate the effect of time on the dissolution of the Al³⁺ and Si⁴⁺ matrix from CFA. Ageing times ranging from 6 to 48 h were studied using the optimum concentration of 1.5 M NaOH. FTIR analysis of the dried CFA residuals after different times, with CFA as a reference, is shown in Fig. 2. The band occurring at 930 cm⁻¹ was associated with symmetric stretching of Al–O and Si–O (Fernández-Jiménez & Palomo, 2005; Musyoka et al., 2012; Mokgehle et al., 2019a). Additionally, it was also noted that these stretches appeared sharper and slightly shifted towards higher frequencies compared to CFA (Fig. 2), as observed for the 48-h peak. This suggested that the incorporation of Na⁺ into the CFA aluminosilicate from the dissolution, NaOH, matrix influenced the asymmetric stretching of Al–O and Si–O (Mokgehle et al., 2019a). Hence, the 48-h ageing time was taken as the optimum and used in subsequent experiments. Experiments conducted for longer than 48 h resulted in damage to the base of the polypropylene bottle.

In Table 1, the XRF data comparing the percentage composition of elements in the residual product as a function of time is shown. Lower percentages of Al₂O₃ were observed in the CFA residues after 48 h in comparison to CFA (Table 1). This indicated that during ageing, Al initially present on the mullite phase of CFA dissolved into the NaOH-activating agent solution (Mokgehle et al., 2019a). Similar

Fig. 1 Concentration of Al³⁺ and Si⁴⁺ at different NaOH concentrations. (Experimental conditions; reaction duration — 24 h, temperature — 50 °C, mass of CFA — 15 g, volume of NaOH — 50 mL)

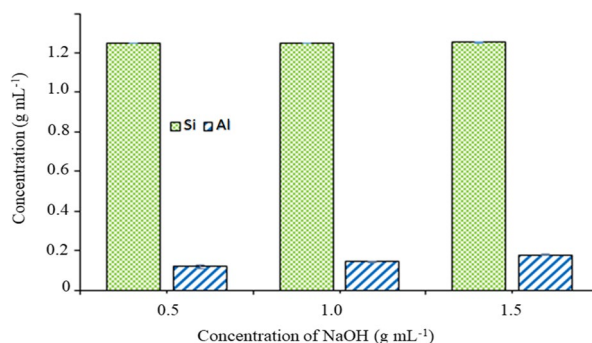


Fig. 2 FTIR spectra of residual products as time was varied

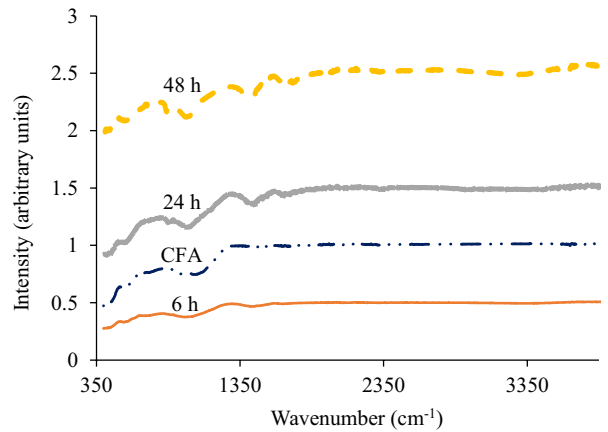


Table 1 XRF data for the effect of time on the dissolution of the aluminosilicate layer of CFA

Metal oxide	CFA	6 h	24 h	48 h
MgO	0.86	0.75	0.84	0.81
SiO ₂	34.9	29.8	30.5	32.5
Al ₂ O ₃	29.0	22.9	22.9	22.4
P ₂ O ₅	0.47	0.29	0.32	0.34
K ₂ O	0.87	0.69	0.66	0.62
CaO	10.5	8.63	10.3	10.7

studies reporting on the dissolution of the aluminium containing mullite phase into NaOH were reported by Joseph et al. (2020), Monasterio-Guillot et al. (2020), Ren et al. (2020), and Cao et al. (2021). Therefore, a higher dissolution of the aluminosilicate layer occurred at 48 h and was in agreement with the data presented in Fig. 2.

Fig. 3 Concentration of Al and Si for three different volumes of NaOH. (Experimental conditions; reaction duration — 48 h, temperature — 50 °C, mass of CFA — 15 g, concentration of NaOH — 1.5 M)

Effect of Volume of NaOH on the Dissolution of the Aluminosilicate Matrix of CFA Studies were performed to investigate the effect of volume of NaOH used for the dissolution of Al³⁺ and Si⁴⁺ from CFA. As the volumes of 1.5 M NaOH increased from 30 to 100 mL, a proportional increase of Al³⁺ was observed, while concentrations of Si⁴⁺ generally remained the same (Fig. 3). Therefore, this indicated that more of the aluminosilicate matrix dissolved into solution when a larger volume of NaOH was used (Kaze et al., 2018; Mokgehle et al., 2019a, b, Kuenzel & Ranjbar, 2019). Therefore, the 100-mL volume of 1.5 M NaOH was the optimum.

FTIR studies on the CFA dried residual products evaluating the effect of volume are shown in Fig. 4. Bands at 930 cm⁻¹ associated with Al–O and Si–O were most intense for the residual where 100 mL of NaOH was used (Mokgehle et al., 2019b). This indicated that the inclusion of Na⁺ from the NaOH-activating agent, into the aluminosilicate layer of the CFA matrix, influenced the asymmetric stretching of

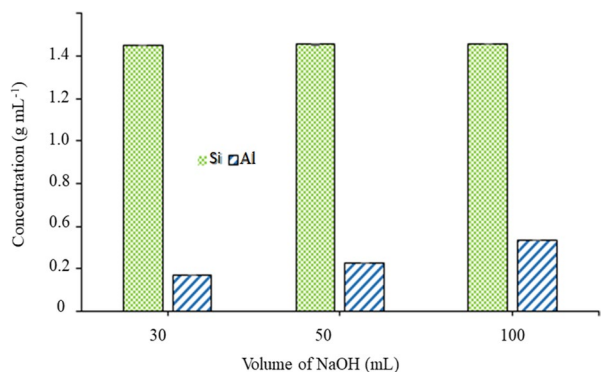
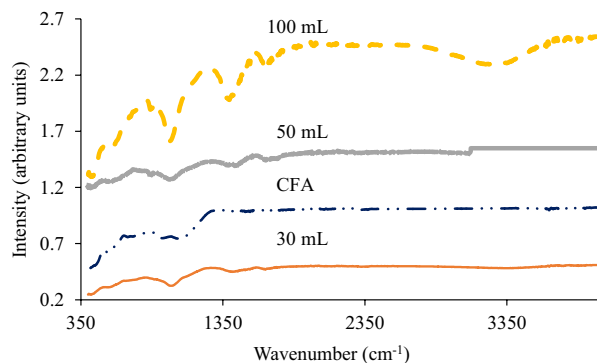


Fig. 4 FTIR spectra of CFA residual products where the effect of volume of NaOH was evaluated



Al–O and Si–O (Mokgehle et al., 2019a, b). Hence, the residue corresponding to when 100 mL of NaOH was used was observed as the optimum and is in consensus with the results from the FAAS studies in Fig. 3.

3.1.2 Crystallization Studies

Effect of Time, Temperature and Variation in Water Content on Crystallization An evaluation on the effect of crystallization on time was performed at 6, 24, 48 and 72 h. Bands associated with Al–O and Si–O symmetric stretching at 930 cm^{-1} appeared to be most intense for 72 h. This indicated that more of the glassy phase present in CFA reacted with the alkaline activator (NaOH) to form zeolite as time was increased as shown in Fig. 5a. Therefore, the optimum time was 72 h.

A subsequent study was done investigating the effect of temperature performed at 35 °C, 120 °C and 200 °C for 72 h. At 35 °C, the Al–O and Si–O symmetric stretching vibrations at 930 cm^{-1} appeared to be almost non-existent compared to the residue crystallized at 120 and 200 °C (Fig. 5b). This indicated that the dissolved glassy phase (from CFA) present in the NaOH alkaline solution failed to effectively form the aluminosilicate gel and eventually crystallize into zeolite at lower temperatures (Wałek et al., 2008; Musyoka et al., 2012; Mokgehle et al., 2019a; Kobayashi et al., 2020). Hence, the optimal temperature for zeolite crystallization was 200 °C.

Thereafter, the analysis on the water content of zeolite crystallization was examined at $\text{H}_2\text{O}/\text{SiO}_2=0$, $\text{H}_2\text{O}/\text{SiO}_2=1$, $\text{H}_2\text{O}/\text{SiO}_2=2$ corresponding to additions of 0, 7.5 and 10 mL of ultra-pure

water to 15 mL slurry, respectively. The most intense peak for Al–O and Si–O asymmetric vibrations was observed at a $\text{H}_2\text{O}/\text{SiO}_2=1$. This suggested that water addition improved the conversion of the CFA glassy phase matrix to zeolite, by forming a super-saturated medium which subsequently allowed for more of the NaOH dissolved Si^{4+} and Al^{3+} species to crystallize on the ash surface (Tajunnisa et al., 2017; Mokgehle et al., 2019a, b; Lu et al., 2021). However, when larger amounts of water are added, the formation of the zeolite crystals is interrupted (Mokgehle et al., 2019a). Therefore, the optimal result was $\text{H}_2\text{O}/\text{SiO}_2=1$.

3.2 Adsorption Studies

3.2.1 Effect of Mass of Zeolite

Adsorption studies were performed to evaluate the effect of mass of zeolite. Batch adsorption studies were performed on different amounts of zeolites (10–80 mg) with 5 mL of 0.5 mg L^{-1} of chromium solution for 180 min each. In Fig. 6, it is shown that as the mass of zeolite was increased, the percentage removal of chromium increased. This suggested that larger doses of zeolite resulted in a larger surface area for adsorption of larger amounts. A similar effect was reported by Saranya et al. (2017), Mokgehle et al. (2019b), Bai et al. (2020), and Qiu et al. (2020). The adsorption capacities for the 10, 20, 40, 60 and 80 mg zeolites were 0.245, 0.100, 0.058, 0.035 and 0.025 mg g^{-1} , respectively. Hence for further studies, 80 mg of zeolite was used as the optimum dose for removing Cr.

Fig. 5 **a** FTIR spectra of zeolites residues synthesized at different time intervals. **b** FTIR spectra for zeolite residues synthesized at different temperatures. **c** FTIR spectra for zeolites synthesized with different solid/liquid ratios

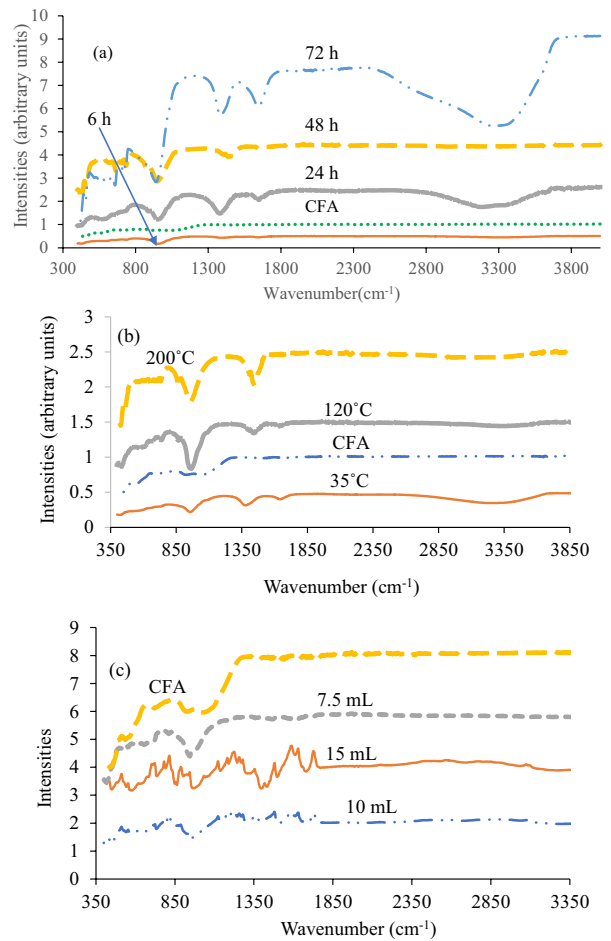
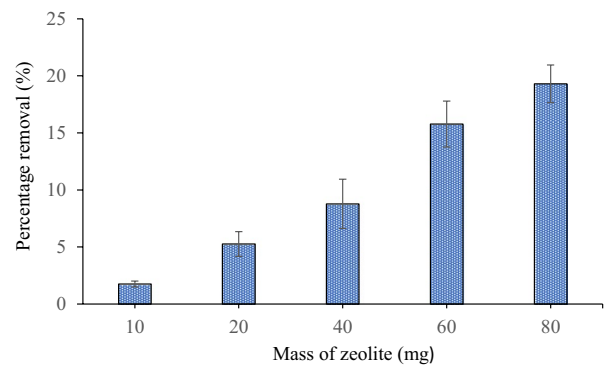


Fig. 6 Percentage removal of chromium while varying mass of zeolite used in batch adsorption studies (experimental conditions; concentration of chromium — 0.5 g mL⁻¹ Cr, contact time — 3 h, temperature — 25 °C)

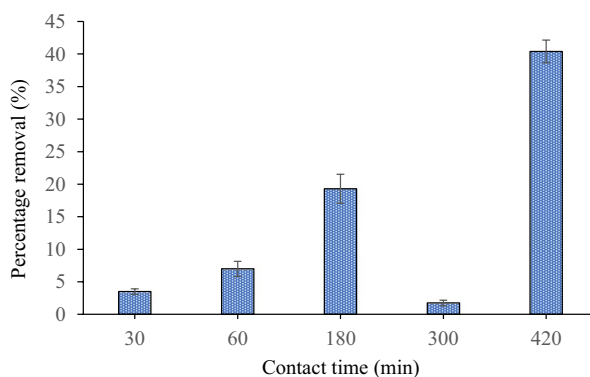


3.2.2 Effect of Contact Time

Batch adsorption studies were performed to evaluate the effect of contact time on zeolite. Adsorption studies were performed using 80 mg of zeolite, with 5 mL of 0.5 mg L⁻¹ of chromium solution at different

contact times (30–420 min). From Fig. 7, a general trend of an increased percentage removal of Cr was observed as contact time was increased. This revealed that at lower contact times many adsorption sites on the zeolite structure were left unoccupied; however, with an increase in the adsorption period, more of

Fig. 7 Percentage removal of chromium at various contact times (experimental conditions; mass of zeolite — 80 mg, concentration of chromium — 0.5 mg L^{-1} , temperature — $25 \text{ }^\circ\text{C}$)



these available sites were filled by Cr. This trend was also reported by Saranya et al. (2017) and Bai et al. (2020). Therefore, 420 min was applied as the optimum time for future studies. The low removal percentages at 300 min could probably be due to agglomeration of the zeolite in solution, preventing its dispersion and subsequent availability of sites for adsorption (Dhiman & Sharma, 2019; Javadian et al., 2020).

3.2.3 Effect of Concentration

Adsorption studies were performed to evaluate the effect of the concentration of chromium on adsorption. Batch adsorption studies were performed at different concentrations of chromium from 0.1 to 0.9 mg L^{-1} . From Fig. 8, a proportional increase in percentage removal of chromium was observed with increasing concentration. This suggested that mass transfer could have been influential during adsorption under these conditions. A large initial chromium concentration provided a large driving force for chromium sorption onto the zeolite surface via cation exchange, as seen for the 0.9-mg L^{-1} study (Fig. 8).

Fig. 8 Percentage removal of chromium at different chromium concentrations (experimental conditions; mass of zeolite — 80 mg, contact time — 7 h, temperature — $25 \text{ }^\circ\text{C}$)

Furthermore, at initial concentrations of 0.7 and 0.9 mg L^{-1} , the removal of Cr showed a tendency of flattening out due possibly to exhaustion of available adsorption sites. This was in agreement with what was observed by Kulkarni et al. (2018) and Hayati et al. (2018). Therefore, 0.9 g mL^{-1} was the optimum concentration.

3.2.4 Effect of Temperature

Adsorption studies were performed to evaluate the effect of temperature on the adsorption of Cr(VI). The temperatures studied ranged from 25 to $75 \text{ }^\circ\text{C}$ with 80 mg of zeolite and 5 mL of 0.9 mg L^{-1} chromium solution for 420 min each. As temperature was increased, the percentage removal of chromium was observed to also increase (Fig. 9). This indicated that there was an increase in the uptake capacity of chromium by the zeolite as the temperature rose from $25 \text{ }^\circ\text{C}$. This suggested that the adsorption process was endothermic in nature. This increased capacity was probably due to the increased number of binding sites that may have been generated by firstly the possible breakage of some internal bonds near the surface of

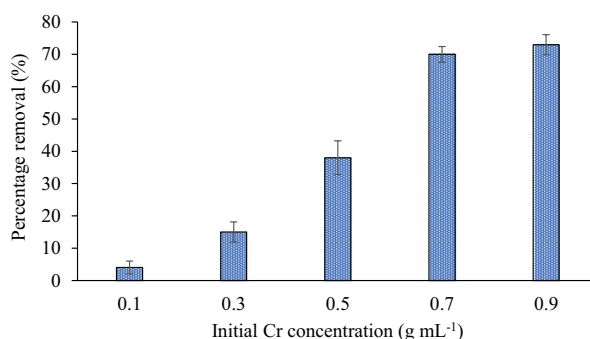


Fig. 9 Percentage removal of chromium after adsorption under a variety of temperatures (experimental conditions; mass of zeolite — 80 mg, contact time — 7 h, initial chromium concentration — 0.9 mg L^{-1})

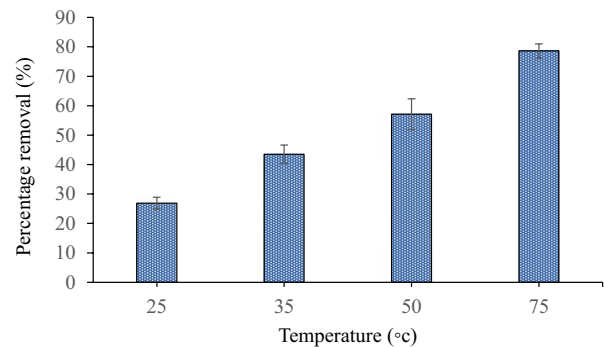


Table 2 Some of the heavy metals detected using ICP-OES in the influent and effluent at the Thulamela water treatment site

	Heavy metal concentration (mg L^{-1})				
	Cr	Fe	Mn	Hg	Se
Influent	-	0.792	0.074	0.012	0.025
Effluent	-	0.028	0.020	0.009	0.007
Removal (%)	-	96.46	72.97	25.00	72.00

binding sites and secondly due to the increased collision frequency by the adsorbate onto the adsorption sites (Saini & Melo, 2013; Vijayalakshmi et al., 2017). Therefore, $75 \text{ }^\circ\text{C}$ was identified as the optimum temperature in this study.

3.3 Application Studies

Application studies were conducted on water collected from the Thulamela Municipality wastewater treatment site, as shown in Table 2. Analysis of chromium in the wastewater samples revealed concentrations that were lower than the limit of detection. This suggested that Cr contamination was unlikely as the Cr effluent concentration was well below the regulatory threshold set by the WHO 2013. Besides Cr, other heavy metals were detected which included Fe, Hg, Mn and Se. The removal percentage in increasing order was as follows: $\text{Hg} < \text{Se} < \text{Fe}$.

4 Conclusion

CFA-derived zeolites were shown to be efficient for the removal of heavy metals from wastewater. CFA-derived zeolites were synthesized based on the hydrothermal treatment method. The optimum conditions

for ageing was a concentration of 1.5 M, at a time of 48 h and NaOH volume of 100 mL. Thereafter, crystallization studies yielded optimum conditions at 72 h, temperature of $200 \text{ }^\circ\text{C}$ and $\text{H}_2\text{O}/\text{SiO}_2 = 1$. Characterization of the synthesized zeolites indicated symmetric stretching of Al–O and Si–O due to the incorporation of Na^+ into the CFA aluminosilicate layer, indicating zeolite formation. XRF data showed that the SiO_2 and Al_2O_3 content was highest in the zeolite synthesized for 48 h. The optimum conditions from the batch adsorption studies were mass = 80 mg, contact time = 420 min, influent Cr concentration = 0.9 M and temperature of $75 \text{ }^\circ\text{C}$, where removal percentages improvements of 77% were obtained from the first to the last optimization study. The optimised batch adsorption parameters were then applied for the removal of chromium and other selected heavy metals in tap water from the Thulamela municipality. Though the removal of chromium could not be determined during application studies, based on ICP-OES studies, CFA-derived zeolites were efficient in the removal of Fe, Mn, Hg and Se with percentage removals of 96.46, 72.97, 25.00 and 72.00%, respectively. Furthermore, ICP-OES analysis indicated that the concentration of chromium was below the detection limit, signifying that the tap water from the studied municipality was adequately treated.

Acknowledgements The University of Venda is thanked.

Author Contribution TMM and NTT conceived the study. TMM and FBN conducted the experiments and data analyses. NTT and TMM supervised the project. TMM and NTT helped to draft the manuscript. All authors read and approved the final manuscript.

Funding The authors were financially supported by the National Research Foundation and Sasol Inzalo.

Data Availability (Data Transparency) Not applicable

Code Availability (Software Application or Custom Code) Not applicable

Declarations

Competing Interests The authors declare no competing interests.

References

- Alguacil, F. J., Alonso, M., Lopez, F., & Lopez-Delgado, A. (2008). Uphill permeation of Cr (VI) using Hostarex A327 as ionophore by membrane-solvent extraction processing. *Chemosphere*, 72, 684–689. <https://doi.org/10.1016/j.chemosphere.2008.02.030>
- Bai, C., Wang, L., & Zhu, Z. (2020). Adsorption of Cr (III) and Pb (II) by graphene oxide/alginate hydrogel membrane: Characterization, adsorption kinetics, isotherm and thermodynamics studies. *International Journal of Biological Macromolecules*, 147, 898–910. <https://doi.org/10.1016/j.ijbiomac.2019.09.249>
- Bakshi, A., & Panigrahi, A. K. (2018). A comprehensive review on chromium induced alterations in fresh water fishes. *Toxicology Reports*, 5, 440–447. <https://doi.org/10.1016/j.toxrep.2018.03.007>
- Bansal, N., Coetzee, J. J., & Chirwa, E. M. (2019). In situ bioremediation of hexavalent chromium in presence of iron by dried sludge bacteria exposed to high chromium concentration. *Ecotoxicology and Environmental Safety*, 172, 281–289. <https://doi.org/10.1016/j.ecoenv.2019.01.094>
- Bashir, A., Malik, L. A., Ahad, S., Manzoor, T., Bhat, M. A., Dar, G. N., & Pandith, A. H. (2019). Removal of heavy metal ions from aqueous system by ion-exchange and biosorption methods. *Environmental Chemistry Letters*, 17, 729–754. <https://doi.org/10.1007/s10311-018-00828-y>
- Buba, M., & Maina, M. (2020). Assessment of physicochemical parameters and some selected heavy metals; cadmium, chromium, iron and lead in borehole water and hand dug well water: A case study of jiwa village in the outskirt of Abuja, Nigeria. *Asian Journal of Science and Technology*, 11, 10751–10756.
- Cao, P., Li, G., Jiang, H., Zhang, X., Luo, J., Rao, M., & Jiang, T. (2021). Extraction and value-added utilization of alumina from coal fly ash via one-step hydrothermal process followed by carbonation. *Journal of Cleaner Production*, 323, 129174. <https://doi.org/10.1016/j.jclepro.2021.129174>
- Chang, S., Kwon, D., & Kim, J. (2020). new approach with fluidized bed reactor using low-cost pyrophyllite/alumina composite membrane for real-metal plating wastewater treatment. in *frontiers in water-energy-nexus—nature-based solutions. Advanced Technologies and Best Practices for Environmental Sustainability* (pp. 177–178). Springer, Cham.
- Chen, Q., Yao, Y., Li, X., Lu, J., Zhou, J., & Huang, Z. (2018). Comparison of heavy metal removals from aqueous solutions by chemical precipitation and characteristics of precipitates. *Journal of Water Process Engineering*, 26, 289–300. <https://doi.org/10.1016/j.jwpe.2018.11.003>
- Crist, R. H., Martin, J. R., & Crist, D. R. (2002). Heavy metal uptake by lignin: Comparison of biotic ligand models with an ion-exchange process. *Environmental Science & Technology*, 36, 1485–1490. <https://doi.org/10.1021/es011136f>
- Deepak, T., Sanjay, G. B., & Shivakumar, C. S. (2021). Acute toxicity of hexavalent chromium on behavioural parameters and histopathology damages in freshwater common carp, *Cyprinus carpio*. *Asian Journal of Research in Zoology*, 2021, 1–8. <https://doi.org/10.9734/ajriz/2021/v4i330114>
- Dhiman, N., & Sharma, N. (2019). Batch adsorption studies on the removal of ciprofloxacin hydrochloride from aqueous solution using ZnO nanoparticles and groundnut (Arachis hypogaea) shell powder: A comparison. *Indian Chemical Engineer*, 61, 67–76. <https://doi.org/10.1080/00194506.2018.1424044>
- Doabi, S. A., Karami, M., Afyuni, M., & Yeganeh, M. (2018). Pollution and health risk assessment of heavy metals in agricultural soil, atmospheric dust and major food crops in Kermanshah province, Iran. *Ecotoxicology and Environmental Safety*, 163, 153–164. <https://doi.org/10.1016/j.ecoenv.2018.07.057>
- Dong, L., Hou, L. A., Wang, Z., Gu, P., Chen, G., & Jiang, R. (2018). A new function of spent activated carbon in BAC process: Removing heavy metals by ion exchange mechanism. *Journal of Hazardous Materials*, 359, 76–84. <https://doi.org/10.1016/j.jhazmat.2018.07.030>
- DWAF DoWAAf. (1996). South African water quality guidelines, vol 1, 2nd edn. Domestic Water Use Department of Water Affairs and Forestry, Pretoria.
- Edokpayi, J. N., Enitan, A. M., Mutileni, N., & Odiyo, J. O. (2018). Evaluation of water quality and human risk assessment due to heavy metals in groundwater around Muledane area of Vhembe District, Limpopo Province, South Africa. *Chemistry Central Journal*, 12, 1–16. <https://doi.org/10.1186/s13065-017-0369-y>
- Edwards, K. C., Kim, H., & Vincent, J. B. (2020). Release of trivalent chromium from serum transferrin is sufficiently rapid to be physiologically relevant. *Journal of Inorganic Biochemistry*, 202, 1–35. <https://doi.org/10.1016/j.jinorgbio.2019.110901>
- Farouk, M., Slibi, D. A., Abd El-Fattah, Z. M., Atallah, M., El-Sherbiny, M. A., & Hassan, M. A. (2020). Effect of SiO₂ addition on chromium transitions in borate glasses. *Silicon*, 13, 1–8. <https://doi.org/10.1007/s12633-020-00649-1>
- Feng, Y., Yang, S., Xia, L., Wang, Z., Suo, N., Chen, H., Long, Y., Zhou, B., & Yu, Y. (2019). In-situ ion exchange electrocatalysis biological coupling (i-IEEBC) for simultaneously enhanced degradation of organic pollutants and heavy metals in electroplating wastewater. *Journal of Hazardous Materials*, 364, 562–570. <https://doi.org/10.1016/j.jhazmat.2018.10.068>
- Fernández-Jiménez, A., & Palomo, A. (2005). Composition and microstructure of alkali activated fly ash binder: Effect of the activator. *Cement and Concrete Research*,

- 35, 1984–1992. <https://doi.org/10.1016/j.cemconres.2005.03.003>
- Fu, Y., Wang, L., Chi, X., Alvarado-Cesar, F., An, N., Song, Y., Wu, J., Zhang, P., & Guo, C. (2020). Body-clearable chromium nitride for synergetic photothermal and photodynamic treatment. *New Journal of Chemistry*, 44, 20039–20046. <https://doi.org/10.1039/D0NJ03943H>
- Hayati, B., Maleki, A., Najafi, F., Gharibi, F., McKay, G., Gupta, V. K., Puttaiah, S. H., & Marzban, N. (2018). Heavy metal adsorption using PAMAM/CNT nanocomposite from aqueous solution in batch and continuous fixed bed systems. *Chemical Engineering Journal*, 346, 258–270. <https://doi.org/10.1016/j.cej.2018.03.172>
- Huang, C., Tang, C., Wu, Q., & Zhu, Q. (2022). Magnetic MnFe₂O₄/ZnFe-LDH for enhanced phosphate and Cr (VI) removal from water. *Environmental Science and Pollution Research*, 1–11. <https://doi.org/10.1007/s11356-022-20049-9>
- Hwang, C.-L., Vo, D.-H., & Huynh, T.-P. (2020). Physical-microstructural evaluation and sulfate resistance of no-cement mortar developed from a ternary binder of industrial by-products. *Environmental Progress & Sustainable Energy*, 2020, 1–14.
- Inada, M., Eguchi, Y., Enomoto, N., & Hojo, J. (2005). Synthesis of zeolite from coal fly ashes with different silica-alumina composition. *Fuel*, 84, 299–304. <https://doi.org/10.1016/j.fuel.2004.08.012>
- Jalees, M. I., Farooq, M. U., Anis, M., Hussain, G., Iqbal, A., & Saleem, S. (2021). Hydrochemistry modelling: Evaluation of groundwater quality deterioration due to anthropogenic activities in Lahore, Pakistan. *Environment, Development and Sustainability*, 23, 3062–3076. <https://doi.org/10.1007/s10668-020-00703-3>
- Javadian, H., Ruiz, M., & Sastre, A. M. (2020). Response surface methodology based on central composite design for simultaneous adsorption of rare earth elements using nanoporous calcium alginate/carboxymethyl chitosan microbicomposite powder containing Ni_{0.2}Zn_{0.2}Fe_{2.6}O₄ magnetic nanoparticles: Batch and column studies. *International Journal of Biological Macromolecules*, 154, 937–953. <https://doi.org/10.1016/j.ijbiomac.2020.03.131>
- Joseph, I. V., Tosheva, L., & Doyle, A. M. (2020). Simultaneous removal of Cd (II), Co (II), Cu (II), Pb (II), and Zn (II) ions from aqueous solutions via adsorption on FAU-type zeolites prepared from coal fly ash. *Journal of Environmental Chemical Engineering*, 8, 103895. <https://doi.org/10.1016/j.jece.2020.103895>
- Kaze, C. R., Djobo, J. N. Y., Nana, A., Tchakoute, H. K., Kamseu, E., Melo, U. C., ..., & Rahier, H. (2018). Effect of silicate modulus on the setting, mechanical strength and microstructure of iron-rich aluminosilicate (laterite) based-geopolymer cured at room temperature. *Ceramics International*, 44, 21442–21450. <https://doi.org/10.1016/j.ceramint.2018.08.205>
- Khan, R., Saxena, A., Shukla, S., Sekar, S., Senapathi, V., & Wu, J. (2021). Environmental contamination by heavy metals and associated human health risk assessment: a case study of surface water in Gomti River Basin, India. *Environmental Science and Pollution Research*, 1–12. <https://doi.org/10.1007/s11356-021-14592-0>
- Kobayashi, Y., Ogata, F., Nakamura, T., & Kawasaki, N. (2020). Synthesis of novel zeolites produced from fly ash by hydrothermal treatment in alkaline solution and its evaluation as an adsorbent for heavy metal removal. *Journal of Environmental Chemical Engineering*, 8, 1–6. <https://doi.org/10.1016/j.jece.2020.103687>
- Kuenzel, C., & Ranjbar, N. (2019). Dissolution mechanism of fly ash to quantify the reactive aluminosilicates in geopolymerisation. *Resources, Conservation and Recycling*, 150, 104421. <https://doi.org/10.1016/j.resconrec.2019.104421>
- Kulkarni, K., Bhogale, G. M., & Nalawade, R. (2018). Adsorptive removal of fluoride from water samples using Azospirillum biofertilizer and lignite. *Korean Journal of Chemical Engineering*, 35, 153–163. <https://doi.org/10.1007/s11814-017-0254-3>
- Kurwadkar, S., Kanel, S. R., & Nakarmi, A. (2020). Groundwater pollution: Occurrence, detection, and remediation of organic and inorganic pollutants. *Water Environment Research*, 92, 1659–1668. <https://doi.org/10.1002/wer.1415>
- Lei, C., Chen, T., Zhang, Q. Y., Long, L. S., Chen, Z., & Fu, Z. P. (2020). Remediation of lead polluted soil by active silicate material prepared from coal fly ash. *Ecotoxicology and Environmental Safety*, 206, 111409. <https://doi.org/10.1016/j.ecoenv.2020.111409>
- Loock-Hattingh, M. M. (2016). Cr(VI) contamination of aqueous systems. Thesis (PhD) Potchefstroom campus: North-West University.
- Lu, P., Ghosh, S., Dorneles de Mello, M., Kamaluddin, H. S., Li, X., Kumar, G., Duan, K., Abeykoon, M., Boscoboinik, A., Qi, L., Dai, H., Luo, T., Al-Thabaiti, S., Narasimharao, K., Khan, Z., Rimer, J. D., Bell, A. T., Dauenhauer, P., Mkhoyan, A., & Tsapatsis, M. (2021). Few-unit-cell MFI zeolite synthesized using a simple di-quatery ammonium structure-directing agent. *Angewandte Chemie*, 133, 19363–19370. <https://doi.org/10.1002/ange.202104574>
- Maitlo, A. A., Jatoti, W. B., Memon, A. F., Soomro, A. H., & Bhayo, M. S. (2021). Assessment of zinc, lead, chromium, and cobalt in commonly consumed herbal medicines in Sindh, Pakistan. *Biological Trace Element Research*, 199, 2366–2374. <https://doi.org/10.1007/s12011-020-02339-w>
- Mokgehle, T. M., Gitari, W. M., & Tavengwa, N. T. (2019b). Synthesis of di-carboxylic acid functionalized zeolites from coal fly ash for Cd (II) removal from acid mine drainage using column studies approach. *Journal of Environmental Chemical Engineering*, 7, 1–36. <https://doi.org/10.1016/j.jece.2019.103473>
- Mokgehle, T. M., Richards, H., Chimuka, L., Gitari, W. M., & Tavengwa, N. T. (2019a). Sulphates removal from AMD using CFA hydrothermally treated zeolites in column studies. *Minerals Engineering*, 141, 1–10. <https://doi.org/10.1016/j.mineng.2019.105851>
- Monasterio-Guillot, L., Alvarez-Lloret, P., Ibañez-Velasco, A., Fernandez-Martinez, A., Ruiz-Agudo, E., & Rodriguez-Navarro, C. (2020). CO₂ sequestration and simultaneous zeolite production by carbonation of coal fly ash: Impact on the trapping of toxic elements. *Journal of CO₂ Utilization*, 40, 101263. <https://doi.org/10.1016/j.jcou.2020.101263>
- Musyoka, N. M., Petrik, L. F., Hums, E., Baser, H., & Schwieger, W. (2012). In situ ultrasonic monitoring

- of zeolite A crystallization from coal fly ash. *Catalysis Today*, 190, 38–46. <https://doi.org/10.1016/j.cattod.2012.03.023>
- Nguyen, T. H., & Lee, M. S. (2018). A review on separation of gallium and indium from leach liquors by solvent extraction and ion exchange. *Mineral Processing and Extractive Metallurgy Review*, 40, 278–291. <https://doi.org/10.1080/08827508.2018.1538987>
- Noah, N. F. M., Sulaiman, R. N. R., Othman, N., Jusoh, N., & Rosly, M. B. (2020). Extractive continuous extractor for chromium recovery: Chromium (VI) reduction to chromium (III) in sustainable emulsion liquid membrane process. *Journal of Cleaner Production*, 247, 119167. <https://doi.org/10.1016/j.jclepro.2019.119167>
- Pakade, V. E., Maremeni, L. C., Ntuli, T. D., & Tavengwa, N. T. (2016). Application of quaternized activated carbon derived from macadamia nutshells for the removal of hexavalent chromium from aqueous solutions. *South African Journal of Chemistry*, 69, 180–188. <https://doi.org/10.17159/0379-4350/2016/v69a22>
- Pakade, V. E., Ntuli, T. D., & Ofomaja, A. E. (2017). Biosorption of hexavalent chromium from aqueous solutions by macadamia nutshell powder. *Applied Water Science*, 7, 3015–3030. <https://doi.org/10.1007/s13201-016-0412-5>
- Park, J. H. (2020). Contrasting effects of Cr (III) and Cr (VI) on lettuce grown in hydroponics and soil: Chromium and manganese speciation. *Environmental Pollution*, 266, 1–7.
- Pohl, A. (2020). Removal of heavy metal ions from water and wastewaters by sulfur containing precipitation agents. *Water, Air and Soil Pollution*, 231(10), 1–17. <https://doi.org/10.1007/s11270-020-04863-w>
- Qiu, Y., Zhang, Q., Gao, B., Li, M., Fan, Z., Sang, W., Hao, H., & Wei, X. (2020). Removal mechanisms of Cr (VI) and Cr (III) by biochar supported nanosized zero-valent iron: Synergy of adsorption, reduction and transformation. *Environmental Pollution*, 265, 1–58. <https://doi.org/10.1016/j.envpol.2020.115073>
- Rahman, Z., & Singh, V. P. (2019). The relative impact of toxic heavy metals (THMs)(arsenic (As), cadmium (Cd), chromium (Cr)(VI), mercury (Hg), and lead (Pb)) on the total environment: An overview. *Environmental Monitoring and Assessment*, 191, 1–21. <https://doi.org/10.1007/s10661-019-7528-7>
- Ren, X., Liu, S., Qu, R., Xiao, L., Hu, P., Song, H., Wu, H., Zheng, C., Wu, X., & Gao, X. (2020). Synthesis and characterization of single-phase submicron zeolite Y from coal fly ash and its potential application for acetone adsorption. *Microporous and Mesoporous Materials*, 295, 109940. <https://doi.org/10.1016/j.micromeso.2019.109940>
- Sadeghi, I., Liu, E. Y., Yi, H., & Asatekin, A. (2019). Membranes with thin hydrogel selective layers containing viral-templated palladium nanoparticles for the catalytic reduction of Cr (VI) to Cr (III). *ACS Applied Nano Materials*, 2, 5233–5244. <https://doi.org/10.1021/acsnm.9b01099>
- Saini, A. S., & Melo, J. S. (2013). Biosorption of uranium by melanin: Kinetic, equilibrium and thermodynamic studies. *Bioresource Technology*, 149, 155–162. <https://doi.org/10.1016/j.biortech.2013.09.034>
- Saleh, T. A., Adio, S. O., Parthasarathy, P., & Danmaliki, G. I. (2020). Scientific insights into modified and non-modified biomaterials for sorption of heavy metals from water. In *Waste Management: Concepts, Methodologies, Tools, and Applications* (pp. 807–827). IGI Global.
- Sanjuán, M. Á., Suarez-Navarro, J. A., Argiz, C., & Estévez, E. (2021). Radiation dose calculation of fine and coarse coal fly ash used for building purposes. *Journal of Radioanalytical and Nuclear Chemistry*, 327, 1045–1054. <https://doi.org/10.1007/s10967-020-07578-8>
- Saranya, N., Nakeeran, E., GiriNandagopal, M. S., & Selvaraju, N. (2017). Optimization of adsorption process parameters by response surface methodology for hexavalent chromium removal from aqueous solutions using *Annona reticulata* Linn peel microparticles. *Water Science and Technology*, 75, 2094–2107. <https://doi.org/10.2166/wst.2017.092>
- Son, E. B., Poo, K. M., Mohamed, H. O., Choi, Y. J., Cho, W. C., & Chae, K. J. (2018). A novel approach to developing a reusable marine macro-algae adsorbent with chitosan and ferric oxide for simultaneous efficient heavy metal removal and easy magnetic separation. *Bioresource Technology*, 259, 381–387. <https://doi.org/10.1016/j.biortech.2018.03.077>
- Sorouraddin, S. M., Farajzadeh, M. A., & Okhravi, T. (2017). Cyclohexylamine as extraction solvent and chelating agent in hexaxation and preconcentration of some heavy metals in aqueous samples based on heat-induced homogeneous liquid-liquid extraction. *Talanta*, 175, 359–365. <https://doi.org/10.1016/j.talanta.2017.07.065>
- Tajunnisa, Y., Sugimoto, M., Sato, T., & Shigeishi, M. (2017). A study on factors affecting geopolymerization of low calcium fly ash. *International Journal of GEOMATE*, 13, 100–107. <https://doi.org/10.21660/2017.36.84153>
- Vijayalakshmi, K., Devi, B. M., Latha, S., Gomathi, T., Sudha, P. N., Venkatesan, J., & Anil, S. (2017). Batch adsorption and desorption studies on the removal of lead (II) from aqueous solution using nanochitosan/sodium alginate/microcrystalline cellulose beads. *International Journal of Biological Macromolecules*, 104, 1483–1494. <https://doi.org/10.1016/j.ijbiomac.2017.04.120>
- Vu, D. H., Bui, H. B., Bui, X. N., An-Nguyen, D., Le, Q. T., Do, N. H., & Nguyen, H. (2020). A novel approach in adsorption of heavy metal ions from aqueous solution using synthesized MCM-41 from coal bottom ash. *International Journal of Environmental Analytical Chemistry*, 100, 1226–1244. <https://doi.org/10.1080/03067319.2019.1651300>
- Watek, T. T., Saito, F., & Zhang, Q. (2008). The effect of low solid/liquid ratio on hydrothermal synthesis of zeolites from fly ash. *Fuel*, 87, 3194–3199. <https://doi.org/10.1016/j.fuel.2008.06.006>
- Wang, Y., Wang, X., Wang, L., Cheng, G., Zhang, M., Xing, Y., Zhao, X., Liu, Y., & Liu, J. (2021). Mitophagy induced by mitochondrial function damage in chicken kidney exposed to Cr (VI). *Biological Trace Element Research*, 199, 703–711. <https://doi.org/10.1007/s12011-020-02176-x>
- Whiteside, M., & Herndon, J. M. (2018). Coal fly ash aerosol: Risk factor for lung cancer. *Journal of Advances in Medicine and Medical Research*, 25, 1–10. <https://doi.org/10.9734/JAMMR/2018/39758>

- World Health Organization. (2003). The World health report: 2003: Shaping the future. World Health Organization.
- World Health Organization. (2006). *Guidelines for drinking-water quality, addendum to volume1: Recommendations* (3rd ed.). World Health Organization.
- Xiaodong, Y., Yongshan, W., Yulin, Z., Feng, H., Zebin, Y., Jun, H., Hailong, W., Yong, S. O., Yinshan, J., & Bin, G. (2019). Surface functional groups of carbon-based adsorbents and their roles in the removal of heavy metals from aqueous solutions: A critical review. *Chemical Engineering Journal*, 366, 608–621. <https://doi.org/10.1016/j.cej.2019.02.119>
- Xie, J., Wang, Z., Wu, D., & Kong, H. (2014). Synthesis and properties of zeolite/hydrated iron oxide composite from coal fly as efficient adsorbent to simultaneously retain cationic and anionic pollutants from water. *Fuel*, 116, 71–76. <https://doi.org/10.1016/j.fuel.2013.07.126>
- Xie, Y., Lin, J., Liang, J., Li, M., Fu, Y., Wang, H., Tu, S., & Li, J. (2019). Hypercrosslinked mesoporous poly (ionic liquid)s with high density of ion pairs: Efficient adsorbents for Cr (VI) removal via ion-exchange. *Chemical Engineering Journal*, 378, 122107. <https://doi.org/10.1016/j.cej.2019.122107>
- Ye, Z., Yin, X., Chen, L., He, X., Lin, Z., Liu, C., Ning, S., Wang, X., & Wei, Y. (2019). An integrated process for removal and recovery of Cr (VI) from electroplating wastewater by ion exchange and reduction–precipitation based on a silica-supported pyridine resin. *Journal of Cleaner Production*, 236, 117631. <https://doi.org/10.1016/j.jclepro.2019.117631>
- Zhang, Z., Cao, H., Song, N., Zhang, L., Cao, Y., & Tai, J. (2020). Long-term hexavalent chromium exposure facilitates colorectal cancer in mice associated with changes in gut microbiota composition. *Food and Chemical Toxicology*, 138, 1–9. <https://doi.org/10.1016/j.fct.2020.111237>
- Zhao, N., Yin, Z., Liu, F., Zhang, M., Lv, Y., Hao, Z., Pan, G., & Zhang, J. (2018). Environmentally persistent free radicals mediated removal of Cr (VI) from highly saline water by corn straw biochars. *Bioresource Technology*, 260, 294–301. <https://doi.org/10.1016/j.biortech.2018.03.116>
- Zhu, S., Huang, X., Yang, X., Peng, P., Li, Z., & Jin, C. (2020). Enhanced transformation of Cr (VI) by heterocyclic-N within nitrogen-doped biochar: Impact of surface modulatory persistent free radicals (PFRs). *Environmental Science & Technology*, 54, 8123–8132. <https://doi.org/10.1021/acs.est.0c02713>

Publisher's Note Springer Nature remains neutral with regard to jurisdictional claims in published maps and institutional affiliations.